


Photoacoustic imaging of living mice enhanced with a low-cost contrast agent

SHUANGYANG ZHANG,^{1,2}  LI QI,^{1,2,3} XIPAN LI,¹ JIAMING LIU,¹
SHIXIAN HUANG,¹ JIAN WU,¹ RUIYUAN LIU,¹ YANQIU FENG,¹
QIANJIN FENG,¹ AND WUFAN CHEN^{1,4}

¹Guangdong Provincial Key Laboratory of Medical Image Processing, School of Biomedical Engineering, Southern Medical University, Guangzhou, Guangdong, 510515, China

²These authors contributed equally to this work

³qili@smu.edu.cn

⁴chenwf@smu.edu.cn

Abstract: One of the advantages of photoacoustic imaging (PAI) is that its image contrast may come from exogenous agents. Such advantage leads to the development of a great number of exogenous probes. However, the biosafety of most of these contrast agents has not yet been confirmed, thus hindering their clinical translation. In this work, we report on the utilization of a clinically commonly used nutritional medicine, the Intralipid, as a new contrast agent for photoacoustic imaging. Intralipid consists of soybean oil, lecithin and glycerin and has long been adapted in clinical practices, mainly as a parenteral nutrition. In our study, we found that with Intralipid, the imaging sensitivity of PAI can be effectively enhanced, as demonstrated in *in vivo* imaging of different organs of nude mice. Further imaging studies on cancerous mice showed not only a twofold PA signal enhancement, but also a strong and long-lasting signal aggregation in the tumor region. Our result revealed the potential of Intralipid to be used in clinical PAI applications, since it is clinically safe, and can be easily prepared at very low cost.

© 2019 Optical Society of America under the terms of the [OSA Open Access Publishing Agreement](#)

1. Introduction

Photoacoustic imaging, also named optoacoustic imaging, is an emerging biomedical imaging technology that combines the high contrast of optical imaging with the high spatial resolution of ultrasound [1]. In PAI, laser illumination is generally used to induce rapid thermoelastic expansion in the tissue volume that produces ultrasonic signals, the amplitude of which is proportional to the absorbed optical intensity. An image that maps the original optical energy deposition inside the target is formed by detecting and processing the ultrasonic signals [2]. Therefore, the image contrast of PAI is either based on endogenous light absorbers, such as hemoglobin or melanin, or from an exogenous contrast agent, which usually provides better contrast than endogenous absorbers by designing its specific absorption spectra. Moreover, exogenous contrast agents could be engineered to deliver additional functionality such as molecular targeting [3–6]. PAI has been successfully used in a wide variety of imaging scenarios in both pre-clinical and human studies, including tumor screening [7–10].

In recent years, a great assortment of exogenous agents have been explored for enhancing PAI image contrast, these include fluorescent molecular probes, nanoparticles, chromogenic substrates and genetic reporters, etc. [11,12]. However, the biosafety of almost all of the above agents has not yet been approved, therefore seriously hindered their clinical translation. At present, a few numbers of exogenous agents (mainly organic dyes) are FDA-approved for used in clinical trials involving photoacoustic imaging, e.g. indocyanine green (ICG) and methylene blue (MB). However, the cost of these dyes is relatively high and their biosafety has not yet been fully evaluated. For example, the use of ICG may cause shock, allergies and other symptoms

[13]. MB in low doses (<2 mg/kg) is safe, however it can induce severe adverse effects such as arrhythmias, coronary vasoconstriction, and hemolytic anemia in patients with renal insufficiency or after administration of higher doses [14,15]. Therefore, a low-cost, clinically safe contrast agent is desirable for future PAI clinical application.

In this paper, we found that a low-cost, clinically widely used medicine, the Intralipid, could be used as a contrast agent for PAI to enhance the imaging sensitivity and contrast. As an emulsion of soybean oil, lecithin and glycerin [16], Intralipid is clinically used as a parenteral nutrition that provides extra energy and amino acids to the body [17]. During clinical practice, its daily dosage should not exceed 2.5 g of fat/kg of body weight (12.5 ml/kg for 20% Intralipid and 25 ml/kg for 10% Intralipid) [18]. In addition, Intralipid can also be used to treat cardiac arrest caused by local anesthesia poisoning [19,20]. In bio-optical imaging research, Intralipid is commonly used as a medium for making tissue-mimicking phantoms because the propagation of light in Intralipid solutions behaves like tissue [16]. However, to our best knowledge, no previous research indicates Intralipid can be used as a contrast agent for photoacoustic imaging. In this work, we found that Intralipid might be used to effectively enhance the imaging signal of PAI in living animal. We first measured the optical and photoacoustic properties of Intralipid solutions under different illumination wavelength. Then, *in vivo* healthy nude mice imaging experiments based on a photoacoustic tomography system were carried out, and significant image intensity increase were observed, further enabling an extended imaging depth. Moreover, Intralipid was tested on cancer-bearing mice. The imaging results not only showed an increase in structural visibility, but also strong PA signal aggregation in the tumor area. Quantitative analysis of the imaging results showed a nearly twofold signal enhancement, consolidating the effectiveness of Intralipid. Our research revealed the potential of Intralipid for clinical PAI applications, such as the screening of breast cancer. A faster clinical translation of PAI is possible with Intralipid because comparing to ICG and other photoacoustic probes, it is not only easier to prepare and has much lower cost, but also much safer.

2. Experimental

The experimental setup, as shown in Fig. 1, relies on a commercial small animal multispectral photoacoustic tomography system (MSOT inVision128, iThera Medical, Germany). Pulsed laser (670 nm - 960 nm tunable) excites the sample through a ten-arm fiber bundle, which provides a homogeneous, 360-degree illumination over the surface of the sample. A special animal holder with a transparent plastic membrane is used for animal positioning. The resulting acoustic waves are simultaneously detected by a ring of ultrasound transducers consisting of 128 elements arranged over an azimuthal span of 270-degrees around the cylinder. The transducers were cylindrically shaped, creating a cross-sectional imaging field of view. The center frequency of the transducer is 5 MHz. The transducer time series signals are then reconstructed into 2D pressure maps using the Back-projection algorithm [21].

All animal experiments were approved by the local Animal Ethics Committee of Southern Medical University and were performed in accordance with current guidelines. In the *in vivo* animal imaging experiment, 8 healthy nude mice (12-15 g/each, female, Southern Medical University, Guangzhou, China), and 2 nude mice carrying 4T1 mammary carcinoma (Southern Medical University Cancer Institute, Guangzhou, China) were used.

Prior to imaging, nude mice were induced with 3% isoflurane and then wrapped in polyethylene membrane and placed in the animal holder with supine position. An insulin injection needle was embedded into the tail vein in advance, and was connected to a long Polyethylene Tubing 10 (PE 10) that enabled Intralipid injection from outside the imaging chamber. After completing the above operations, the mice were then transferred to an imaging chamber filled with water at 34 degrees Celsius. All nude mice were anesthetized with 1% isoflurane during imaging. Mice were allowed to stabilize within the imaging chamber for approximately 15 minutes prior to imaging.

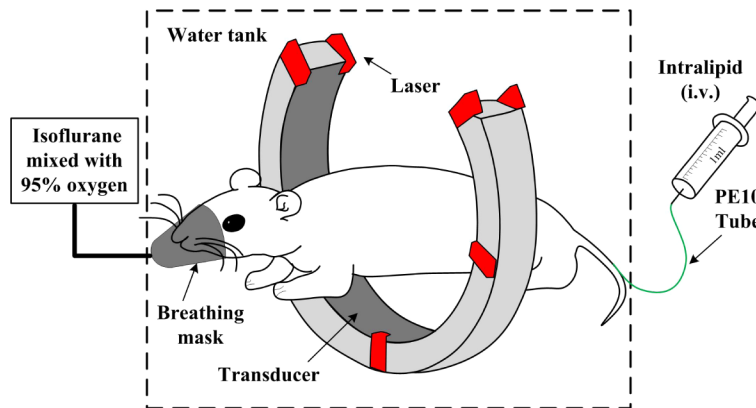


Fig. 1. Schematic of the PAT system.

After a 60 mins pre-injection scan, every two healthy nude mice were respectively injected with 0.9% physiological saline solution (10 ml/kg), 10% Intralipid (10 ml/kg), 20% Intralipid (10 ml/kg) and 50 ug/ml ICG (10 ml/kg) within a time period of ~120 s. Two nude mice with 4T1 tumor were injected with 20% Intralipid (10ml/kg). To evaluate the sensitivity of Intralipid, three different tissue regions: head, abdomen, and tumor were imaged. For each region, multispectral PAT imaging were performed at seven different illumination wavelengths: 730, 760, 780, 800, 820, 850 and 875 nm. The laser energy at the above wavelengths were 59.08 mJ, 61.17 mJ, 60.54 mJ, 60.1 mJ, 59.5 mJ, 57.95 mJ and 57.01 mJ, respectively. The laser irradiation covered an area of about 4 cm², so the maximum surface energy density was about 15.5 mJ/cm², which was below the maximum permissible exposure (MPE) of 25 mJ/cm² recommended by the American National Standards Institute (ANSI) [22]. Before image reconstruction, the photoacoustic raw data was normalized to laser energy to avoid errors due to fluctuations in laser energy. Pre-injection scans were imaged for 1 hour and post-injection scans were imaged for 3 hours, both at 5 minutes intervals. For image reconstructions in these experiments, the speed of sound in the medium was set to 1536 m/s and the reconstruction images were consisted of 600×600 pixels.

3. Results

3.1. The photoacoustic property of Intralipid

As a first step, the photoacoustic and optical absorption properties of Intralipid solution was examined. In this experiment, 3 solutions (saline, 10% Intralipid, and 20% Intralipid) were separately loaded into a 5 ml Eppendorf (EP) tube. These solutions were fixed on a phantom holder and placed in the imaging chamber of the described PAT system for cross-sectional imaging. Figure 2(a) shows the sensitivity of different concentrations of Intralipid and physiological saline at different wavelengths. The PA signal intensity was normalized in the region inside the EP tube. Moreover, the near-infrared absorption characteristics of these solutions were further measured with an absorption spectrometer. The optical absorption spectra of the above three solutions are shown in Fig. 2(b). Even though the optical absorption of saline was near zero, it still had a very weak PA signal that is larger than zero. This is because the photoacoustic signal has a signal floor, and the measured saline PA signal intensity was almost the same to that of the water surrounding the EP tube. As can be seen, for both optical absorption and PA intensity, Intralipid is much stronger than saline solution, and 20% Intralipid is stronger than 10% Intralipid.

In addition, the PA signals of 20% Intralipid, ICG at two different concentration and fresh blood collected from nude mice were compared. In clinical use, the dosage of ICG should be

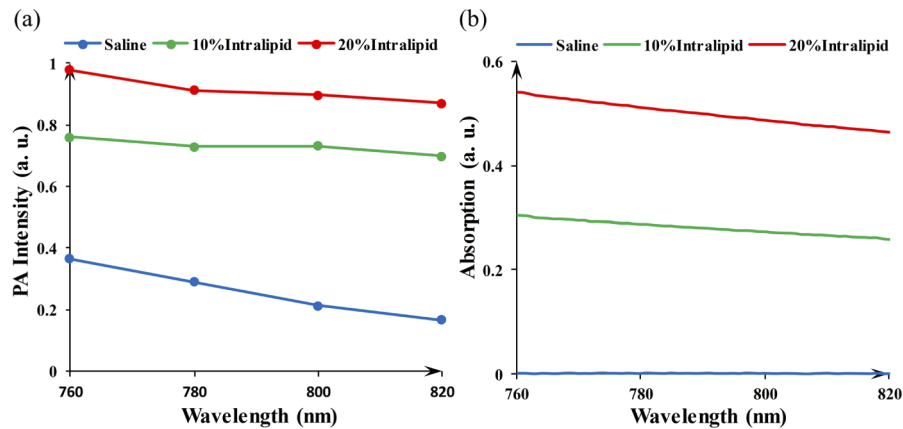


Fig. 2. (a) The PA intensity of physiological saline solution, 10% Intralipid and 20% Intralipid at different wavelengths, as measured by the described PAT imaging system. (b) The absorption spectra of saline solution, 10% Intralipid and 20% Intralipid.

0.5 mg of ICG/kg of body weight [23]. The injection amount used in our animal studies was 10 ml/kg, so the maximum concentration of ICG was calculated to be 50 ug/ml. The quantitative analysis results are listed in Table 1. The results showed that the PA signal of the fresh blood was very strong and its intensity was about 40 times that of 20% Intralipid. In addition, 20% Intralipid had very close PA signal intensity as that of ICG with a concentration of 0.5 ug/ml. The PA signal of the ICG at the maximum dose allowed in the clinic did not exceed the photoacoustic signal of fresh blood.

Table 1. PA signal intensity of different materials (a. u.)

Material	Wavelengths			
	760 nm	780 nm	800 nm	820 nm
Blood	3622.3 ± 153.29	3654.52 ± 157.16	3780.25 ± 92.66	3804.71 ± 170.27
ICG 50 ug/ml	3253.34 ± 185.48	3465.18 ± 199.02	3250.2 ± 196.89	2641.74 ± 150.68
ICG 0.5 ug/ml	85.35 ± 3.2	80 ± 5.2	80.86 ± 3.09	77.61 ± 2.02
20% Intralipid	84.62 ± 19.55	68.09 ± 11.11	62.59 ± 12.28	67.05 ± 12.38

3.2. Healthy nude mice study

Next, we performed *in vivo* small animal experiment with healthy nude mice. Figure 3 shows the PAT image before and after 20% Intralipid injection on one of the healthy animal. Figure 3(a) and (d) were images acquired before injection at $t = -5$ min, and Fig. 3(b) and (e) were acquired after injection at $t = 175$ min. The difference images, Fig. 3(c) and (f), were obtained by subtracting the pre-injection image from the post-injection image. As can be seen in the head imaging results (see online supporting information, Head Visualization 1), before Intralipid injection, the contrast between the head region and the background was poor: the jugular vein, the posterior ear vein and the sagittal sinus blood vessels could hardly be seen and the boundary brain was not clear. After the injection of Intralipid (Fig. 3(b)), the vascular signal had been obviously enhanced and the brain boundary became distinct. PA signal around the bottom region of the head was recovered (red arrow), indicating an enhanced imaging depth. The difference image in Fig. 3(c) showed a large intensity enhancement inside the brain, which also suggested that Intralipid can increase photoacoustic imaging depth. In the results of the abdomen region (Fig. 3(d), Online

supporting information, Abdomen [Visualization 2](#)), the overall contrast of the pre-injection scan image was relatively low, and the boundary between the renal cortex and the renal medulla were not evident and the intestine was completely blurred. After Intralipid injection (Fig. 3(e)), the external contours of kidney were much clearer and the intestinal signal was enhanced. Also, the subcutaneous blood vessels became visible while in the pre-injection image they were too weak to be recognized. Notice that the background of the difference image was around 0, proving that the sensitivity enhancement was not related to the imaging system, but was caused by the injection of Intralipid.

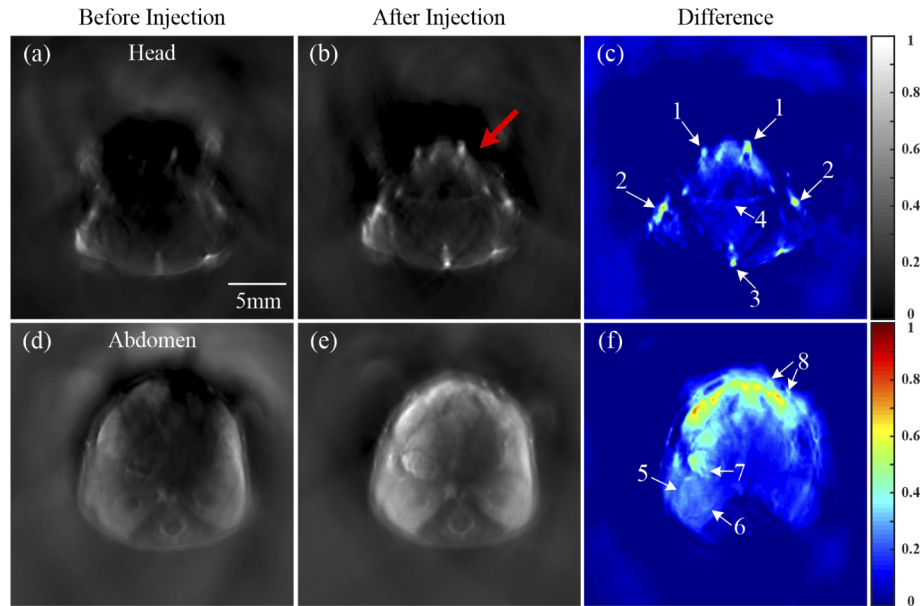


Fig. 3. PAT images of the head and abdomen of healthy nude mice, before and after injection of 20% Intralipid. Arrows 1: jugular vein, 2: posterior ear vein, 3: the sagittal sinus, 4: the brain boundary, 5: renal cortex, 6: renal medulla, 7: intestine, and 8: subcutaneous blood vessels. Illumination wavelength: 760 nm. See online supporting information, Head [Visualization 1](#) and Abdomen [Visualization 2](#).

As a result of the quantitative analysis, Fig. 4 shows the head PA intensity time series with and without the injection of saline solution, 10% Intralipid and 20% Intralipid. Pre-injection scans and post-injection scans at 5 minutes intervals were selected to quantify the dynamic changes of PA signals. As can be seen from the graph, before injection, the PA intensities of each group are stable and there are no significant differences between the groups. After injecting Intralipid, the PA intensity was significantly increased, with 10% and 20% Intralipid increased by $71.98\% \pm 13.24\%$ and $112.98\% \pm 29.98\%$, respectively, while after the injection of saline, the PA intensity remained unchanged. Moreover, even 3 hours after the injection of Intralipid, the PA signal was still increasing, indicating a slow metabolic rate of Intralipid in the body.

3.3. Cancerous nude mice imaging study

Next, *in vivo* tumor-bearing small animal imaging study was carried out. Figure 5 and online supporting information, Tumor [Visualization 3](#) show the PAT imaging results by injecting 20% Intralipid on one of the mice. Figure 5(a) was acquired at $t = -5$ min before injection and Fig. 5(b) was at $t = 175$ min after injection. The difference image Fig. 5(c) is obtained by subtracting the images before and after injection. As can be seen, before injection, there was hardly any intensity

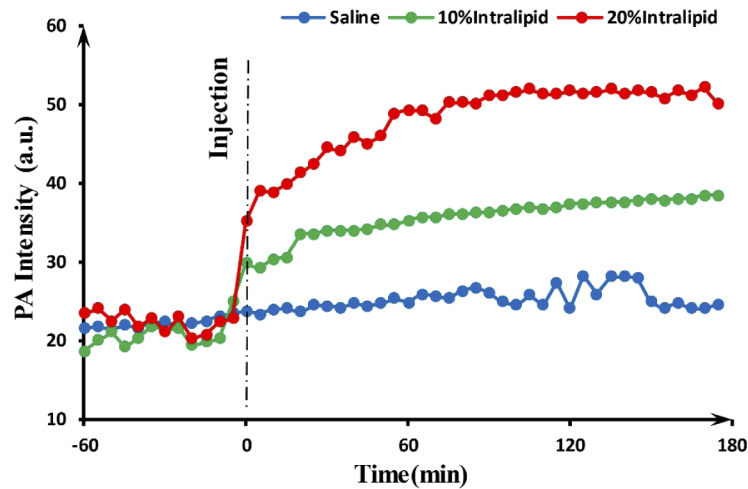


Fig. 4. Head PA intensity curve with saline solution, 10% Intralipid and 20% Intralipid. Time dependent PA intensity values were averaged from signals within the head area.

difference between tumor and normal tissue, and the contrast and boundary of the tumor region was poor. After Intralipid injection, an overall PA signal enhancement was observed within the animal, including both tumorous and normal tissues, but the signal increase inside the tumor region was more distinct. Moreover, the difference image showed that Intralipid had strong aggregation around the tumor surface (red arrow), which is usually vessel-rich, while in normal tissues, only the blood vessels had comparable enhancement. Furthermore, the PA intensity at different time was measured at both the tumor region and normal tissue, and the result was shown in Fig. 5(d). Before injection, there was no significant difference in PA intensity between normal tissue and tumor area. However, after Intralipid injection, the PA intensity of tumor area rapidly increased by 57.67% around the first few minutes, and it kept on rising until reaching a 125.98% increase at $t = 175$ min. These results indicated that Intralipid might be used to enhance tumor recognition and detection.

3.4. Statistical analysis

A statistical analysis of all the *in vivo* animal experiments was performed. For each organ region, 6 images acquired at different time points were selected for quantification from the pre-injection and post-injection scans respectively. All the images were normalized to the same scale according to the background (mainly water absorption). Figure 6 shows the statistical analysis of the head and the abdomen from all 6 healthy nude mice, the data were derived from the mean PA intensities of the whole tissue regions (the whole mouse body part) and therefore represents the overall signal enhancement of the contrast agent. As can be seen, the PA intensity of all our studies had a significant increase after Intralipid injection ($p < 0.0001$). For the head area, an average PA intensity enhancement of $68.69\% \pm 13.62\%$ and $111.96\% \pm 31.7\%$ were obtained by the injection of 10% and 20% Intralipid respectively. For the abdomen region, the PA intensity was increased by $70.53\% \pm 5.78\%$ by 20% Intralipid, and $36.37\% \pm 3.39\%$ by 10% Intralipid.

Figure 7 shows the results of PA signal changes of different organs. The data of each organ were derived from the mean PA intensities of the regions of interest (sagittal sinus: a small region around arrow 3 in Fig. 3; normal tissue: tissue area other than the tumor in Fig. 5; kidney: the left and right kidney region in Fig. 3; tumor: the tumor region in Fig. 5). After injection of 20% Intralipid, the sagittal sinus had the most significant enhancement of PA signal with an average increase of $126.91\% \pm 15.39\%$. In fact, in the head region, major vasculatures including the

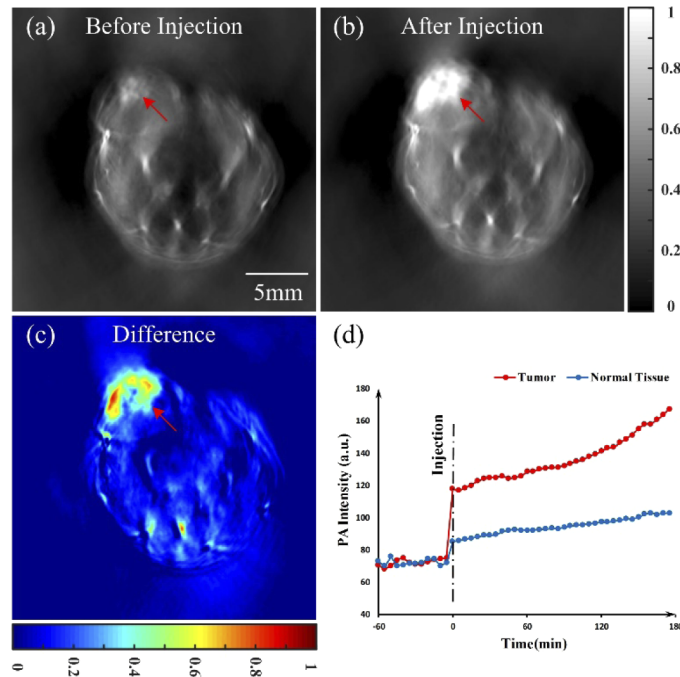


Fig. 5. PAT images of nude mouse bearing 4T1 tumor. (d) shows the PA intensity curves at tumor region and normal tissue. Time dependent PA intensity values were calculated as the mean intensity within normal tissue and tumor regions. Illumination wavelength: 760 nm. See online supporting information, Tumor [Visualization 3](#).

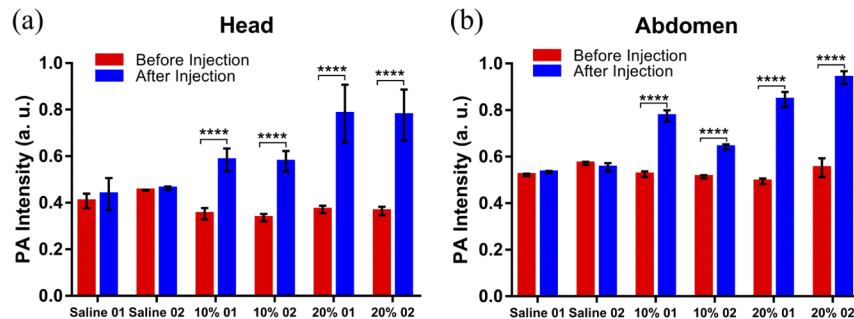


Fig. 6. Statistical analysis of (a) head, (b) abdomen from all 6 healthy nude mice. Serial numbers 01 and 02 indicates two mice injected with the same solution.

sagittal sinus, the jugular vein, and the posterior ear vein all shown obvious PA signal increase, as can be seen in Fig. 3. The tumor area had the second strongest PA signal enhancement of $116.54\% \pm 5.87\%$. Also can be seen in Fig. 5, the PA signal enhancement effect in the vascular-rich area inside the tumor was most obvious and concentrated, followed by several large blood vessels in the abdomen. This might indicate that Intralipid preferentially enhanced the vascular-rich or rapid metabolism regions. Finally, an average PA signal increase of $69.09\% \pm 17.19\%$ in normal tissue, and $25.88\% \pm 3.82\%$ in kidney were obtained, showing an observable enhancement brought about by Intralipid.

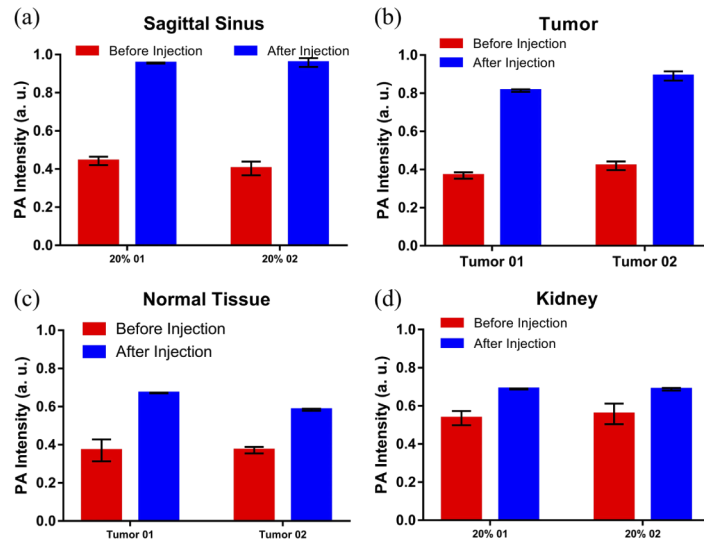


Fig. 7. Statistical analysis of (a) Sagittal sinus, (d) Kidney from healthy nude mice and (b) Tumor, (c) Normal tissue from 2 cancerous mice. Serial numbers 01 and 02 indicates two different mice injected with the same solution (20% Intralipid).

3.5. Comparative study with ICG

As a comparison, *in vivo* nude mice study of ICG injection was performed. The imaging protocol was the same as that of the Intralipid. The head and the abdomen regions of two healthy nude mice were imaged and analyzed. Figure 8 shows the PA signal enhancement of different tissue regions before and after 50 ug/ml ICG injection (maximum clinical dosage) on two healthy animal. The head and abdomen data were derived from the mean PA intensities of the tissue

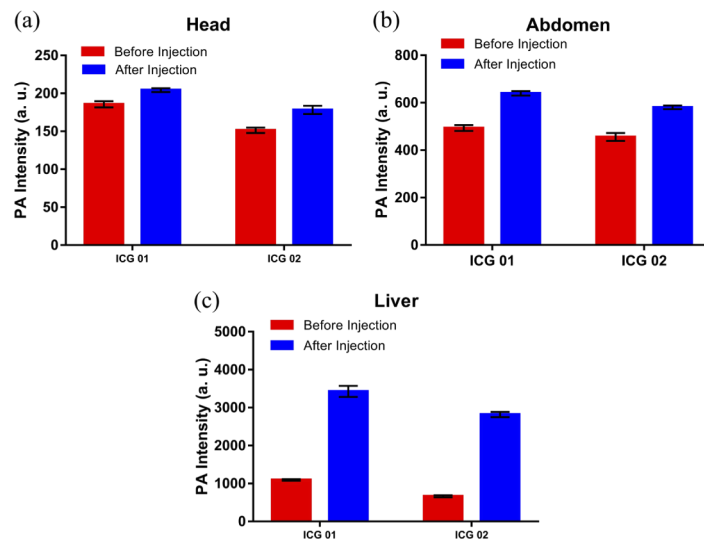


Fig. 8. Statistical analysis of (a) Head, (b) Abdomen and (c) Liver from two healthy animal before and after injection of 50 ug/ml ICG. Serial numbers 01 and 02 indicates two mice injected with 50 ug/ml ICG.

regions (the whole mouse body part). The liver data was derived from the visible liver region within the abdomen cross-section. For each region, 6 images acquired at different time points were selected for quantification from the pre-injection and post-injection scans respectively. For the post-injection data, the images with the strongest PA signal were selected for quantification because ICG clearance is relatively fast. As can be seen from Fig. 8, after the injection of ICG, an average PA intensity enhancement of 13.96% in head area, 28.56% in abdomen region, and 269.52% in liver were obtained. The weak signal enhancement at the head region indicated that only a small amount of ICG entered the head. On the contrary, a large amount of ICG rapidly accumulated in the liver region, leading to a significant increase in PA signals. The signal enhancement at the rest of the abdomen, including the kidney area, were not that obvious. This organ-specific enhancement characteristic of ICG makes it very effective and suitable for liver imaging. However, compared to 20% Intralipid, even though the ICG has a higher maximum signal enhancement, its performance at other regions of the body was limited.

4. Discussions

The above results showed substantial PAI image quality improvement introduced by Intralipid, revealing an attractive prospect for its translation to clinical photoacoustic imaging applications. The advantages of Intralipid as a photoacoustic imaging probe is prominent: it is clinically safe and has been used extensively, can be easily prepared and at very low cost. With our founding, Intralipid could be readily translated to clinical PAI applications such as the screening of breast cancer [9], sentinel lymph nodes metastatic [7], carotid artery atherosclerosis [10] and so on. In addition, although we only studied the performance of Intralipid on a photoacoustic tomography system, it should also be used in other PAI systems such as photoacoustic microscopy (PAM) [24–26], and a similar image quality enhancement is expected.

In the *in vitro* experiments, 20% Intralipid had a relatively weak optical absorption compared to fresh blood and ICG. However, *in vivo* experiments showed that the injection of 20% Intralipid almost doubled the overall PA signal of the whole body. This indicated that the enhancement of PA signals might not only related to light absorption, but also related to the increase of tissue scattering. This is because compared to previous reported PA probes, Intralipid has a strong light scattering property. Therefore, the benefits of Intralipid for PAI might have been brought about not only by its optical absorption, but also by its scattering characteristic, such as in optical coherence tomography [27]. Nonetheless, the mechanism by which Intralipid enhances the quality of PAI is still unclear and requires further investigation.

Compared to the organ-selective enhancement and fast clearance of ICG, Intralipid diffuses in blood slowly, and achieves an overall PA signal enhancement to the whole body. The slow clearance of intralipid might not be a big problem because originally intralipid is a parenteral nutrition that could be safely absorbed by the body. In contrast, this feature makes it suitable for long-term imaging.

Finally, the optical absorption spectrum of Intralipid does not have a sharp peak, therefore it might be difficult to quantitatively determine its spatial distribution with spectral un-mixing methods [28]. However, as demonstrated in this work, one of the features of Intralipid for PAI image enhancement is its increase in overall image quality, which is similar to some previous reported PA probes, e.g. carbon nanotube [3] and polypyrrole nanoparticles [4].

5. Conclusion

As a clinical widely used medicine, the Intralipid has been used in clinical practices either as a parenteral nutrition, or a medication for cardiac arrest. In this work, we found that the Intralipid might also be a promising agent for providing photoacoustic contrast. By conducting *in vitro* and *in vivo* validations, our results showed that the PAI imaging quality could be significantly enhanced by intravenously injected Intralipid, with a maximum twofold signal intensity increase.

Further experiments of tumor-bearing mice showed even a strong and long-lasting PA signal aggregation in the tumor area, revealing the potential of such medicine for cancer diagnosis. Compared to other PAI probes, the advantages of Intralipid is its safety and easy preparation. Therefore, Intralipid has the potential to accelerate clinical translation of PAI technology.

Funding

China Postdoctoral Science Foundation (2017M610536); National Natural Science Foundation of China (31700857, 61471188, 81871437); Guangdong Provincial Natural Science Foundation (2017A030310516); Guangzhou Science and Technology Program (201804010375); Guangdong Key Area R&D Program (2018B030333001).

Disclosures

The authors declare that there are no conflicts of interest related to this article.

References

1. P. Beard, "Biomedical photoacoustic imaging," *Interface Focus* **1**(4), 602–631 (2011).
2. M. Xu and L. V. Wang, "Photoacoustic imaging in biomedicine," *Rev. Sci. Instrum.* **77**(4), 041101 (2006).
3. A. De la Zerda, C. Zavaleta, S. Keren, S. Vaithilingam, S. Bodapati, Z. Liu, J. Levi, B. R. Smith, T. J. Ma, O. Oralkan, Z. Cheng, X. Chen, H. Dai, B. T. Khuri-Yakub, and S. S. Gambhir, "Carbon nanotubes as photoacoustic molecular imaging agents in living mice," *Nat. Nanotechnol.* **3**(9), 557–562 (2008).
4. Z. Zha, Z. Deng, Y. Li, C. Li, J. Wang, S. Wang, E. Qu, and Z. Dai, "Biocompatible polypyrrole nanoparticles as a novel organic photoacoustic contrast agent for deep tissue imaging," *Nanoscale* **5**(10), 4462–4467 (2013).
5. J. Weber, P. C. Beard, and S. E. Bohndiek, "Contrast agents for molecular photoacoustic imaging," *Nat. Methods* **13**(8), 639–650 (2016).
6. S. Roberts, C. Andreou, C. Choi, P. Donabedian, M. Jayaraman, E. C. Pratt, J. Tang, C. Perez-Medina, M. Jason de la Cruz, W. J. M. Mulder, J. Grimm, M. Kircher, and T. Reiner, "Sonophore-enhanced nanoemulsions for optoacoustic imaging of cancer," *Chem. Sci.* **9**(25), 5646–5657 (2018).
7. I. Stoffels, S. Morscher, I. Helfrich, U. Hillen, J. Leyh, N. C. Burton, T. C. Sardella, J. Claussen, T. D. Poeppel, H. S. Bachmann, A. Roesch, K. Griewank, D. Schadendorf, M. Gunzer, and J. Klode, "Metastatic status of sentinel lymph nodes in melanoma determined noninvasively with multispectral optoacoustic imaging," *Sci. Transl. Med.* **7**(317), 317ra199 (2015).
8. F. Knieling, C. Neufert, A. Hartmann, J. Claussen, A. Urlich, C. Egger, M. Vetter, S. Fischer, L. Pfeifer, and A. Hagel, "Multispectral optoacoustic tomography for assessment of Crohn's disease activity," *N. Engl. J. Med.* **376**(13), 1292–1294 (2017).
9. L. Lin, P. Hu, J. Shi, C. M. Appleton, K. Maslov, L. Li, R. Zhang, and L. V. Wang, "Single-breath-hold photoacoustic computed tomography of the breast," *Nat. Commun.* **9**(1), 2352 (2018).
10. I. Ivankovic, E. Mercep, C. G. Schmedt, X. L. Dean-Ben, and D. Razansky, "Real-time Volumetric Assessment of the Human Carotid Artery: Handheld Multispectral Optoacoustic Tomography," *Radiology* **291**(1), 45–50 (2019).
11. V. Ntziachristos and D. Razansky, "Molecular imaging by means of multispectral optoacoustic tomography (MSOT)," *Chem. Rev.* **110**(5), 2783–2794 (2010).
12. X. L. Dean-Ben, S. Gottschalk, B. Mc Larney, S. Shoham, and D. Razansky, "Advanced optoacoustic methods for multiscale imaging of in vivo dynamics," *Chem. Soc. Rev.* **46**(8), 2158–2198 (2017).
13. M. Hope-Ross, L. A. Yannuzzi, E. S. Gragoudas, D. R. Guyer, J. S. Slakter, J. A. Sorenson, S. Krupsky, D. A. Orlock, and C. A. Puliafito, "Adverse reactions due to indocyanine green," *Ophthalmology* **101**(3), 529–533 (1994).
14. P. R. Ginimuge and S. D. Jyothi, "Methylene blue: revisited," *J. Anaesthesiol. Clin. Pharmacol.* **26**(4), 517–520 (2010).
15. L. van Manen, H. J. M. Handgraaf, M. Diana, J. Dijkstra, T. Ishizawa, A. L. Vahrmeijer, and J. S. D. Mieog, "A practical guide for the use of indocyanine green and methylene blue in fluorescence-guided abdominal surgery," *J. Surg. Oncol.* **118**(2), 283–300 (2018).
16. S. T. Flock, S. L. Jacques, B. C. Wilson, W. M. Star, and M. J. van Gemert, "Optical properties of Intralipid: a phantom medium for light propagation studies," *Lasers Surg. Med.* **12**(5), 510–519 (1992).
17. L. M. Hansen, B. Hardie, and J. Hidalgo, "Fat emulsion for intravenous administration: clinical experience with intralipid 10%," *Ann. Surg.* **184**(1), 80–88 (1976).
18. "<https://www.drugs.com/pro/intralipid.html>".
19. L. Rothschild, S. Bern, S. Oswald, and G. Weinberg, "Intravenous lipid emulsion in clinical toxicology," *Scand. J. Trauma Resusc. Emerg. Med.* **18**(1), 51 (2010).
20. G. L. Weinberg, "Lipid Emulsion Infusion Resuscitation for Local Anesthetic and Other Drug Overdose," *Anesthesiology* **117**(1), 180–187 (2012).

21. M. Xu and L. V. Wang, "Universal back-projection algorithm for photoacoustic computed tomography," *Phys. Rev. E: Stat., Nonlinear, Soft Matter Phys.* **71**(1), 016706 (2005).
22. L. I. o. America, "American National Standard for Safe Use of Lasers," Laser Institute of America (2007).
23. "<https://www.drugs.com/international/indocyanine-green.html>."
24. H. F. Zhang, K. Maslov, G. Stoica, and L. V. Wang, "Functional photoacoustic microscopy for high-resolution and noninvasive in vivo imaging," *Nat. Biotechnol.* **24**(7), 848–851 (2006).
25. P. Hai, J. Yao, K. I. Maslov, Y. Zhou, and L. V. Wang, "Near-infrared optical-resolution photoacoustic microscopy," *Opt. Lett.* **39**(17), 5192–5195 (2014).
26. J. Yao, L. Song, and L. V. Wang, "Photoacoustic microscopy: superdepth, superresolution, and superb contrast," *IEEE Pulse* **6**(3), 34–37 (2015).
27. Y. Pan, J. You, N. D. Volkow, K. Park, and C. Du, "Ultrasensitive detection of 3D cerebral microvascular network dynamics in vivo," *NeuroImage* **103**, 492–501 (2014).
28. S. Tzoumas, N. Deliolanis, S. Morscher, and V. Ntziachristos, "Unmixing Molecular Agents From Absorbing Tissue in Multispectral Photoacoustic Tomography," *IEEE Trans. Med. Imaging* **33**(1), 48–60 (2014).